

Symmetry Energy Effects in the Direct Detection of Isospin-Violating Dark Matter

Hao Zheng¹, Zhen Zhang¹ and Lie-Wen Chen^{*1,2}

¹*Department of Physics and Astronomy and Shanghai Key Laboratory for Particle Physics and Cosmology,
Shanghai Jiao Tong University, Shanghai 200240, China*

²*Center of Theoretical Nuclear Physics, National Laboratory of Heavy Ion Accelerator, Lanzhou 730000, China*
(Dated: March 21, 2014)

Isospin-violating dark matter (IVDM) provides a possible mechanism to ameliorate the tension among recent direct detection experiments. For IVDM, we demonstrate that the results of direct detection experiments based on neutron-rich target nuclei may depend strongly on the density dependence of the symmetry energy which is presently largely unknown and controls the neutron skin thickness that reflects the relative difference of neutron and proton distributions in the neutron-rich nuclei. In particular, using the neutron and proton distributions obtained from Skyrme-Hartree-Fock calculations with the symmetry energy constrained by the latest model-independent measurement of the neutron skin thickness of ^{208}Pb from PREX experiment at JLab, we find that for the xenophobic IVDM in the mass region constrained by CMDS-II(Si), the symmetry energy effect may enhance the sensitivity of Xe-based detectors (e.g., XENON100 and LUX) to the DM-proton cross section by a factor of 3, compared with the results using the empirical Helm charge distributions. This symmetry energy effect can even enhance the sensitivity by more than an order of magnitude for the xenophobic IVDM with mass larger than 80 GeV.

I. INTRODUCTION

The possible existence of dark matter (DM) is one of the most intriguing aspects of modern particle physics, astrophysics and cosmology. In order to survey the nature of DM, a number of observations and experiments have been conducted or are underway around the world. The most recent cosmological results based on *Planck* measurements of the cosmic microwave background (CMB) temperature and lensing-potential power spectra indicate that DM comprises about 27% of the energy density of the Universe which also includes about 5% baryon matter and about 68% dark energy [1]. Many theories beyond the Standard Model of particle physics predict natural candidates for DM, e.g., the weakly interacting massive particles (WIMPs) which are a class of hypothetical stable neutral particles, with a huge range in masses from 1 GeV to 100 TeV and interaction cross sections with normal matter (proton) from 10^{-40} to 10^{-50} cm² [2, 3]. In terrestrial laboratory, DM might be directly detected through their elastic scattering off nuclei in particle detectors [4]. A number of underground DM direct detection experiments have been performed, among them an excess of events over the expected background has been observed by CoGeNT [5], DAMA [6] and CRESSTII [7] as well as the recent results presented by the CDMS-II(Si) collaboration [8, 9]. However, these results are in strong tension with the constraints set by some other experimental groups like XENON100 [10, 11], LUX [12] and SuperCDMS(Ge) [13], leaving a confusing situation for the community. This has led a number of attempts trying to explain the discrepancy by considering atomic uncertainties [14] or different mechanisms that deviate from standard assumptions about DM interactions or its astrophysical distributions [15–18].

Isospin-Violating Dark Matter (IVDM) provides a very promising mechanism to reconcile the tension among different experiments [19–25]. Within the IVDM framework, DM is assumed to couple differently with protons and neutrons, and this assumption of the isospin violation has been supported by a number of theoretical works [26–30] based on the particle physics point of view. Many parameters need to be specified in the standard method of analyzing DM direct detection experiments [31] and recently Frandsen *et al.* [32] presented a systematic discussion on the possible ways to ameliorate the tension among different experiments. They found that the tension between the CDMS-II(Si) results and the XENON100 bounds is independent of the astrophysical uncertainties concerning the DM halo and any momentum- and velocity-dependence of the cross section in particle physics, but it can be largely ameliorated or even resolved within the framework of IVDM.

Besides the uncertainties in astrophysics and particle physics concerning the interaction between a DM particle scattering off a single nucleon mentioned above, the uncertainties in nuclear physics describing how the struck nucleon is distributed inside the nucleus may also play an important role in interpreting DM signals. This is because in DM direct detection experiments, the nuclear form factors are generally applied to describe the DM-nucleus cross section and the bounds on DM-nucleon cross section are then obtained accordingly. In particular, the Helm nuclear form

* Corresponding author (email: lwchen@sjtu.edu.cn)

factor extracted from empirical charge distributions [33, 34] has been commonly adopted in current direct detection experiments. However, the DM-nucleus interaction should be in principle described by using the form factors of both proton and neutron distributions in the nuclei rather than the charge distributions since the DM particle actually interacts with the protons and neutrons in the nuclei. Within the framework of relativistic mean field (RMF) theory, Chen *et al.* [35] derived the nuclear form factor for the spin-independent scattering between the WIMPs and nucleus, and they found that the results can deviate from the empirical Helm form factor by 15% to 25% for the whole recoil energy spectrum of $0 \sim 100$ keV. A recent work by Co' *et al.* [36] suggests that the use of different distributions for protons and neutrons instead of the commonly used empirical Helm charge distributions for a target nucleus could be important, especially if IVDM is considered.

For stable nuclei, the proton distribution can be well determined from the charge distribution which can be accurately measured with electron scattering [37–39]. In contrast, the neutron distribution is generally determined from hadron scattering experiments and the results are usually highly model dependent due to the non-perturbative strong interaction [40]. Recently, the Lead Radius Experiment (PREX) collaboration at Jefferson Laboratory (JLab) published their results on the measurement of the parity-violating cross section asymmetry in the elastic scattering of polarized electrons from ^{208}Pb [40], which provides a model-independent probe of neutron density distributions. The PREX measurement leads to a value of $\sqrt{\langle r_n^2 \rangle} = 5.78^{+0.16}_{-0.18}$ fm for the rms radius of the neutron distributions for ^{208}Pb , implying a large neutron skin thickness, i.e., $\Delta r_{\text{np}} = \sqrt{\langle r_n^2 \rangle} - \sqrt{\langle r_p^2 \rangle} = 0.33^{+0.16}_{-0.18}$ fm by assuming a point-proton rms radius of 5.45 fm [41]. One can see that the obtained results of Δr_{np} has a large error, indicating a large uncertainty of the neutron distribution relative to the proton distribution.

Theoretically, it has been established [42, 43] that the Δr_{np} is intimately related to the nuclear matter symmetry energy which characterizes the isospin dependent part of the equation of state (EOS) of asymmetric nuclear matter [44]. In particular, it has been shown recently that the Δr_{np} of heavy nuclei is uniquely determined by the density slope $L(\rho_c)$ of the symmetry energy at a subsaturation cross density $\rho_c \approx 0.11 \text{ fm}^{-3}$ [45]. These features imply that the uncertainties of Δr_{np} , especially the neutron distributions, predicted by various nuclear models are essentially due to our poor knowledge about the symmetry energy. The symmetry energy is of critical importance for understanding not only the structure and reaction of radioactive nuclei, but also a number of interesting issues in astrophysics, such as the structure of neutron stars and the mechanism of supernova explosions, and has become a hot topic in current research frontiers of nuclear physics and astrophysics [46]. The determination of the symmetry energy provides a strong motivation for studying isospin-dependent phenomena with radioactive nuclei at a number of new/planning rare isotope beam facilities around the world, such as CSR/Lanzhou and BRIF-II/Beijing in China, RIBF/RIKEN in Japan, SPIRAL2/GANIL in France, FAIR/GSI in Germany, SPES/LNL in Italy, RAON in Korea, and FRIB/NSCL and T-Rex/TAMU in USA.

In this work, using the proton and neutron distributions obtained from Skyrme-Hartree-Fock calculations with the symmetry energy slope parameter $L(\rho_c)$ constrained by the neutron skin thickness from PREX experiment, we investigate the symmetry energy effects in the direct detection of dark matter. Our results indicate that although the symmetry energy effects on the extracted bounds on DM-nucleon cross sections are negligible in the direct detection for isospin-invariant DM, they could become critically important in the detection for IVDM. In particular, for the xenophobic IVDM in the mass region constrained by CMDS-II(Si), the symmetry energy effect may enhance the sensitivity of Xe-based detectors (e.g., XENON100 and LUX) to the DM-proton cross section by a factor of 3, compared with the results using the empirical Helm nuclear form factors extracted from empirical charge distributions. This symmetry energy effect can even enhance the sensitivity by more than a factor of 10 for the xenophobic IVDM with mass larger than 80 GeV. These features imply that the DM-nucleus scattering could be a useful model-independent tool to determine the neutron distribution in nuclei as well as the symmetry energy if DM is xenophobic IVDM.

This article is organized as follows. In Sec. II we review the general nature of the symmetry energy and the standard way of analyzing DM direct detection experiments. In Sec. III we study the symmetry energy effects on the form factors of various nuclei that are widely used as the target in the direct detection experiments and the DM-proton cross sections relative to the empirical ones. We present our conclusions in Sec. IV.

II. MODELS AND METHODS

A. The symmetry energy and Skyrme-Hartree-Fock approach

The EOS of isospin asymmetric nuclear matter, defined by its binding energy per nucleon, can be well approximated by

$$E(\rho, \delta) = E_0(\rho) + E_{\text{sym}}(\rho)\delta^2 + \mathcal{O}(\delta^4), \quad (1)$$

in terms of baryon density $\rho = \rho_p + \rho_n$ and isospin asymmetry $\delta = (\rho_n - \rho_p)/\rho$ with ρ_p and ρ_n denoting the proton and neutron densities. $E_0(\rho) = E(\rho, \delta = 0)$ corresponds to the EOS of symmetric nuclear matter, and the nuclear symmetry energy can be expressed as

$$E_{\text{sym}}(\rho) = \frac{1}{2!} \frac{\partial^2 E(\rho, \delta)}{\partial \delta^2} \Big|_{\delta=0}. \quad (2)$$

There are no odd-order δ terms in Eq. (1) due to the exchange symmetry between protons and neutrons (isospin symmetry) in nuclear matter. Neglecting the contribution from higher-order terms in Eq. (1) leads to the well-known empirical parabolic law for EOS of asymmetric nuclear matter, which has been verified by all many-body theories to date, at least for densities up to moderate values [44].

Furthermore, around a reference density ρ_r , the symmetry energy $E_{\text{sym}}(\rho)$ can be expanded as

$$E_{\text{sym}}(\rho) = E_{\text{sym}}(\rho_r) + \frac{L(\rho_r)}{3} \left(\frac{\rho - \rho_r}{\rho_r} \right) + \mathcal{O} \left(\frac{\rho - \rho_r}{\rho_r} \right)^2, \quad (3)$$

with

$$L(\rho_r) = 3\rho_r \frac{\partial E_{\text{sym}}(\rho)}{\partial \rho} \Big|_{\rho=\rho_r}. \quad (4)$$

The slope parameter $L(\rho_r)$ characterizes the density dependence of symmetry energy around ρ_r . It has been shown [45] that the neutron skin thickness Δr_{np} of heavy nuclei is uniquely fixed by the density slope $L(\rho_c)$ at a subsaturation cross density $\rho_c \approx 0.11 \text{ fm}^{-3}$ which roughly corresponds to the average density of the nuclei.

For the calculations of finite nuclei, we use in the present work the standard Skyrme-Hartree-Fock (SHF) approach in which the nuclear effective interaction is taken to have a zero-range, density- and momentum-dependent form, i.e. [47],

$$\begin{aligned} V_{12}(\mathbf{R}, \mathbf{r}) = & t_0(1 + x_0 P_\sigma) \delta(\mathbf{r}) \\ & + \frac{1}{6} t_3(1 + x_3 P_\sigma) \rho^\sigma(\mathbf{R}) \delta(\mathbf{r}) \\ & + \frac{1}{2} t_1(1 + x_1 P_\sigma) (K'^2 \delta(\mathbf{r}) + \delta(\mathbf{r}) K^2) \\ & + t_2(1 + x_2 P_\sigma) \mathbf{K}' \cdot \delta(\mathbf{r}) \mathbf{K} \\ & + i W_0 (\sigma_1 + \sigma_2) \cdot [\mathbf{K}' \times \delta(\mathbf{r}) \mathbf{K}], \end{aligned} \quad (5)$$

with $\mathbf{r} = \mathbf{r}_1 - \mathbf{r}_2$ and $\mathbf{R} = (\mathbf{r}_1 + \mathbf{r}_2)/2$. In the above expression, the relative momentum operators $\mathbf{K} = (\nabla_1 - \nabla_2)/2i$ and $\mathbf{K}' = -(\nabla_1 - \nabla_2)/2i$ act on the wave function on the right and left, respectively. The quantities P_σ and σ_i denote, respectively, the spin exchange operator and Pauli spin matrices.

The Skyrme interaction in Eq. (5) includes totally 10 parameters, i.e., the 9 Skyrme force parameters σ , $t_0 - t_3$, $x_0 - x_3$, and the spin-orbit coupling constant W_0 . This standard SHF approach has been shown to be very successful in describing the structure of finite nuclei, especially global properties such as binding energies and charge radii [47–49]. Instead of using directly the 9 Skyrme force parameters, we can express them explicitly in terms of 9 macroscopic quantities, i.e., ρ_0 , $E_0(\rho_0)$, the incompressibility K_0 , the isoscalar effective mass $m_{s,0}^*$, the isovector effective mass $m_{v,0}^*$, $E_{\text{sym}}(\rho_r)$, $L(\rho_r)$, G_S , and G_V . The G_S and G_V are respectively the gradient and symmetry-gradient coefficients in the interaction part of the binding energies for finite nuclei defined as

$$E_{\text{grad}} = G_S (\nabla \rho)^2 / (2\rho) - G_V [\nabla(\rho_n - \rho_p)]^2 / (2\rho). \quad (6)$$

Then, by varying individually these macroscopic quantities within their known ranges, one can examine more transparently the correlation of nuclear matter properties with each individual macroscopic quantity. Recently, this correlation analysis method has been successfully applied to study the neutron skin [45, 50] and giant monopole resonance of finite nuclei [51], the higher-order bulk characteristic parameters of ANM [52], and the relationship between the nuclear matter symmetry energy and the symmetry energy coefficient in the mass formula [53]. In the present work, we use the 9 macroscopic quantities instead of using directly the 9 Skyrme force parameters as shown later. Especially, we study the symmetry energy effects by varying the $L(\rho_c)$ value while keeping the other macroscopic quantities unchanged.

B. General Method of Analyzing DM Direct Detection Experiments

In this work, we use the standard method of analyzing DM direct detection experiments [31, 32]. The spin-independent differential event rate of the nuclear recoils with a recoil energy of E_R , occurred in a detector due to an elastic collision between a target nucleus of mass m_N^A and a DM particle of mass m_χ , can be expressed as

$$\frac{dR^A}{dE_R} = \frac{\rho_\chi N_T^A}{m_N^A m_\chi} \int_{v_{\min}}^{\infty} v_\chi f(v_\chi + \mathbf{v}_E) \frac{d\sigma_p}{dE_R} A^2 |F_A(q)|^2 d^3 v_\chi, \quad (7)$$

where A represents the mass number of the target nucleus and N_T^A is the number of target nucleus per unit mass in the detector, ρ_χ is the local halo DM density, $f(v_\chi)$ is the local DM velocity distribution evaluated in the Galactic rest frame with $v_\chi = |\mathbf{v}_\chi|$, and \mathbf{v}_E is Earth velocity in the Galactic rest frame [54, 55]. $\frac{d\sigma_p}{dE_R}$ and $F_A(q)$ denote the spin-independent differential DM-proton scattering cross-section and the effective form factors, respectively, and they will be detailed below. The $q = (2m_N^A E_R)^{1/2}$ is the momentum transfer between the DM particle and the struck nucleus. The lower limit v_{\min} of the integration in Eq. (7) corresponds to the smallest DM velocity that can give a recoil energy of E_R

$$v_{\min}(E_R) = \sqrt{\frac{m_N^A E_R}{2\mu_A^2}}, \quad (8)$$

where $\mu_A = m_N^A m_\chi / (m_N^A + m_\chi)$ is the DM-nucleus reduced mass.

The total number of events R , characterized by the unit as one event $kg^{-1} d^{-1}$, in a detector consists of compound targets with finite detector energy resolution, is

$$R = \sum_A \eta_A \int dE_R \epsilon(E_R) \text{Res}(E_R) \frac{dR^A}{dE_R}, \quad (9)$$

where η_A is the natural abundance of each isotope A for a compound target, $\epsilon(E_R)$ is the detector efficiency and $\text{Res}(E_R)$ is the detector response function [9, 11]. The E_R integration limits are determined by the energy detection thresholds of the experiments.

It is convenient, and usually adequate, to describe the matter distributions of a finite nucleus by a form factor, F , in analyzing DM direct detection experiments [31]. In the first-order Born approximation, the form factors of spherical nuclei are the Fourier transforms of the proton and neutron density distributions, i.e.,

$$F_A^{p,n}(q) = \int \rho_A^{p,n}(\mathbf{r}) e^{i\mathbf{q} \cdot \mathbf{r}} d^3 r = \frac{4\pi}{q} \int_0^\infty r \sin(qr) \rho_A^{p,n}(r) dr, \quad (10)$$

where index p denotes proton and n denotes neutron, respectively. The density distributions, $\rho_A^{p,n}$, for spherical nuclei can be obtained by using a mean-field approach [56], e.g., the SHF approach as we discussed above.

We further define the so-called effective form factors in Eq. (7) in terms of $F_A^{p,n}$ as

$$|F_A(q)|^2 = \frac{1}{A^2} |ZF_A^p(q) + g_{np} N F_A^n(q)|^2, \quad (11)$$

where Z (N) is the proton (neutron) number of the target nucleus, $A=Z+N$, and $g_{np} = f_n/f_p$ is the isospin-violation factor with f_n and f_p denoting the effective coupling of DM to neutrons and protons, respectively. The spin-independent differential DM-proton scattering cross-section can then be expressed as [32]

$$\frac{d\sigma_p}{dE_R} = \frac{m_N^A \sigma_p}{2\mu_{p\chi}^2 v_\chi^2}, \quad (12)$$

where $\mu_{p\chi}$ is the reduced DM-proton mass, and σ_p is the elastic DM-proton cross-section at zero momentum transfer ($q = 0$). Integrating the differential event rate in Eq. (7) with respect to E_R , e.g., Eq. (9), one can relate the experimental number of scattering events in a direct detection experiment with the DM-proton cross-section σ_p .

However, in experiments usually reported is the DM-nucleon cross section σ_N , rather than σ_p . σ_N is an effective cross section by assuming that the DM particle couples with protons and neutrons equally (i.e., $g_{np} = 1$) and the nuclear form factors are the same for protons and neutrons which are in practice commonly taken as the empirical charge form factors proposed by Helm [33]. Obviously, the DM-proton cross section σ_p is generally different from the

DM-nucleon cross section σ_N , but they can be related to each other by the so-called degradation factors D_p defined as [23]

$$D_p \equiv \frac{\sigma_p}{\sigma_N} = \frac{\sum_A \eta_A N_T^A A^2 \int \epsilon(E_R) \text{Res}(E_R) k(E_R, m_\chi) |F_A(E_R)|^2 dE_R}{\sum_A \eta_A N_T^A A^2 \int \epsilon(E_R) \text{Res}(E_R) k(E_R, m_\chi) |F_A^{\text{Helm}}(E_R)|^2 dE_R}, \quad (13)$$

with

$$k(E_R, m_\chi) = \int_{v_{\min}(E_R, m_\chi)}^{\infty} f(\mathbf{v}_\chi + \mathbf{v}_E) / v_\chi d^3 v_\chi. \quad (14)$$

In Eq. (13), the F_A^{Helm} is the Helm form factor which is obtained by considering a charge density with a Gaussian surface distribution and has the following simple analytical expression

$$F_A^{\text{Helm}}(q) = 3 \frac{j_1(qr_N)}{qr_N} \times e^{-(qs)^2/2}, \quad (15)$$

where j_1 is the first-order spherical Bessel function, r_N is an effective nuclear radius and s is a measure of the nuclear skin thickness. For r_N and s , the following standard parametrization has been used [31]

$$r_N^2 = c^2 + \frac{7}{3} \pi^2 a^2 - 5s^2, \quad (16)$$

$$c \approx 1.23 A^{1/3} - 0.60 \text{ fm}, \quad (17)$$

$$a \approx 0.52 \text{ fm}, \quad (18)$$

$$s \approx 0.9 \text{ fm}. \quad (19)$$

If a DM direct detection experiment reports its results in terms of σ_N , one can then obtain the corresponding results of σ_p from Eq. (13) for any general cases with different g_{np} and nuclear form factors. In this way, one can thus study the isospin-violating effects and the symmetry energy effects simultaneously in analyzing the DM signals.

III. RESULTS AND DISCUSSIONS

A. Symmetry energy effects on nuclear form factors

As mentioned above, the neutron skin thickness of heavy nuclei is uniquely determined by the symmetry energy density slope parameter $L(\rho_c)$ at a subsaturation cross density $\rho_c \approx 0.11 \text{ fm}^{-3}$ [45]. Therefore, the $L(\rho_c)$ parameter controls the relative difference of the neutron and proton distributions in the nuclei. In the present work, we investigate the symmetry energy effects by varying the $L(\rho_c)$ parameter in the SHF calculations to fit the model-independent result of $\Delta r_{np} = 0.33_{-0.18}^{+0.16} \text{ fm}$ for ^{208}Pb from the recent PREX experiment at JLab.

Shown in Fig. 1 is the Δr_{np} of ^{132}Xe as a function of that of ^{208}Pb in SHF calculations with the Skyrme interaction MSL1 [45] by varying $L(\rho_c)$ while keeping the other 8 macroscopic quantities and the spin-orbit coupling constant W_0 fixed at their default values in the MSL1 interaction, namely, $\rho_0 = 0.1586 \text{ fm}^{-3}$, $E_0(\rho_0) = -15.998 \text{ MeV}$, the incompressibility $K_0 = 235.12 \text{ MeV}$, the isoscalar effective mass $m_{s,0}^* = 0.806m$, the isovector effective mass $m_{v,0}^* = 0.706m$, $E_{\text{sym}}(\rho_c) = 26.67 \text{ MeV}$, $G_S = 126.69 \text{ MeV} \cdot \text{fm}^5$, $G_V = 68.74 \text{ MeV} \cdot \text{fm}^5$, and $W_0 = 113.62 \text{ MeV} \cdot \text{fm}^5$. The MSL1 interaction has been obtained by fitting a number of experimental data of finite nuclei, including the binding energy, the charge rms radius, the neutron $3p_{1/2} - 3p_{3/2}$ energy level splitting in ^{208}Pb , isotope binding energy difference, and neutron skin data of Sn isotopes. For comparison, we also include in Fig. 1 the results from SHF calculations with 43 other Skyrme interactions (BSk1, BSk4, BSk5, BSk7, BSk10, BSk14, BS15, Dutta, E-fit, Esigma-fit, Gsigma-fit, KDE, KDE0, MSL0, RATP, Rsigma-fit, SGI, SGII, SK255, SK272, SKa, SkI1, SkI2, SkI5, SKM, SkMP, SKM*, SKT1, SKT4, SKT5, SKT6, Skz0, Skz1, Skz2, Skz3, Skz4, Skz-1, SLy4, SLy5, SLy9, Z-fit, Zsigma-fit, and Zsigma-fit) and RMF calculations from 6 different interaction parameter sets (FSU, IUFSU, TM1, PK1, NL3, and NL1). The references of these Skyrme and RMF interactions can be found in Refs. [57–59]. We have selected these interactions in such a way that their $L(\rho_c)$ values scatter in large region and are not close to another. One can see clearly a nice model-independent linear correlation between the neutron skin thicknesses of ^{208}Pb and ^{132}Xe within the non-relativistic and relativistic models with different interactions. In addition, although there are few interactions that predict a Δr_{np} of ^{208}Pb larger than 0.33 fm measured by the model-independent PREX experiment, one can easily obtain a large Δr_{np} of ^{208}Pb by increasing the $L(\rho_c)$ value in the MSL1 interaction. In

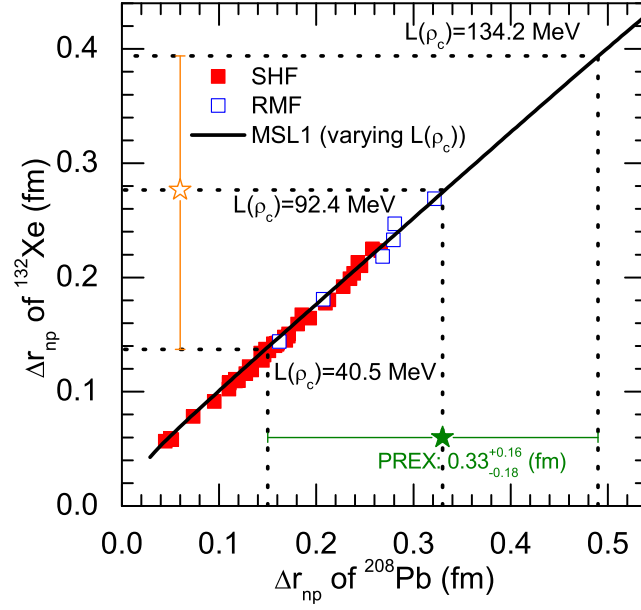


Figure 1: (Color online) Neutron skin thickness for ^{132}Xe vs. that for ^{208}Pb predicted by mean-field models with different interactions. Constraints set by PREX measurement [40] are also shown.

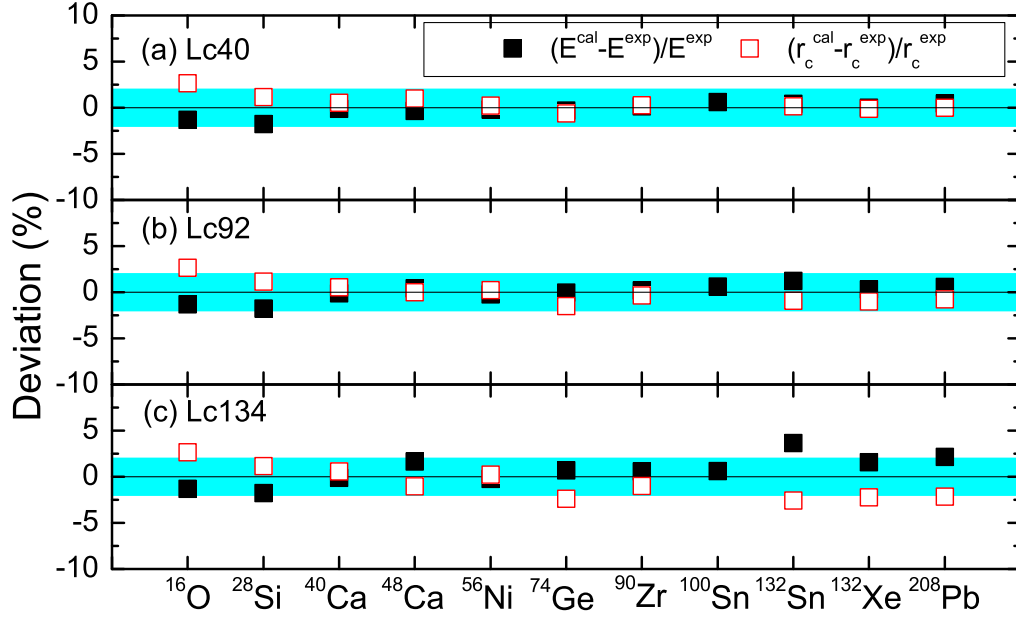


Figure 2: (Color online) Deviations of the binding energies (solid squares) and charge rms radii (open squares) of a number of nuclei obtained from SHF with Lc40, Lc92 and Lc134 from those measured in experiments. The bands indicate a deviation within $\pm 2\%$.

particular, we find a value of $L(\rho_c) = 92.4^{+41.8}_{-51.9}$ MeV in the MSL1 interaction predicts $\Delta r_{\text{np}} = 0.33^{+0.16}_{-0.18}$ fm for ^{208}Pb and $\Delta r_{\text{np}} = 0.28^{+0.12}_{-0.14}$ fm for ^{132}Xe . Therefore, we use $L(\rho_c) = 40.5$ MeV, 92.4 MeV and 134.2 MeV in the MSL1 interaction, denoted as Lc40, Lc92 and Lc134, respectively, to study the symmetry energy effects in the present work. We would like to point out that the large neutron skin thickness for ^{208}Pb measured by the PREX experiment can also be explained within the RMF model [60].

To test the Skyrme parameter sets Lc40, Lc92, and Lc134, we calculate the binding energies and charge rms radii for a number of closed-shell or semi-closed-shell nuclei, i.e., ^{16}O , ^{40}Ca , ^{48}Ca , ^{56}Ni , ^{90}Zr , ^{100}Sn , ^{132}Sn , and ^{208}Pb , as well as the nuclei ^{28}Si , ^{74}Ge , and ^{132}Xe . The elements Si, Ge and Xe are widely used as targets in the DM direct

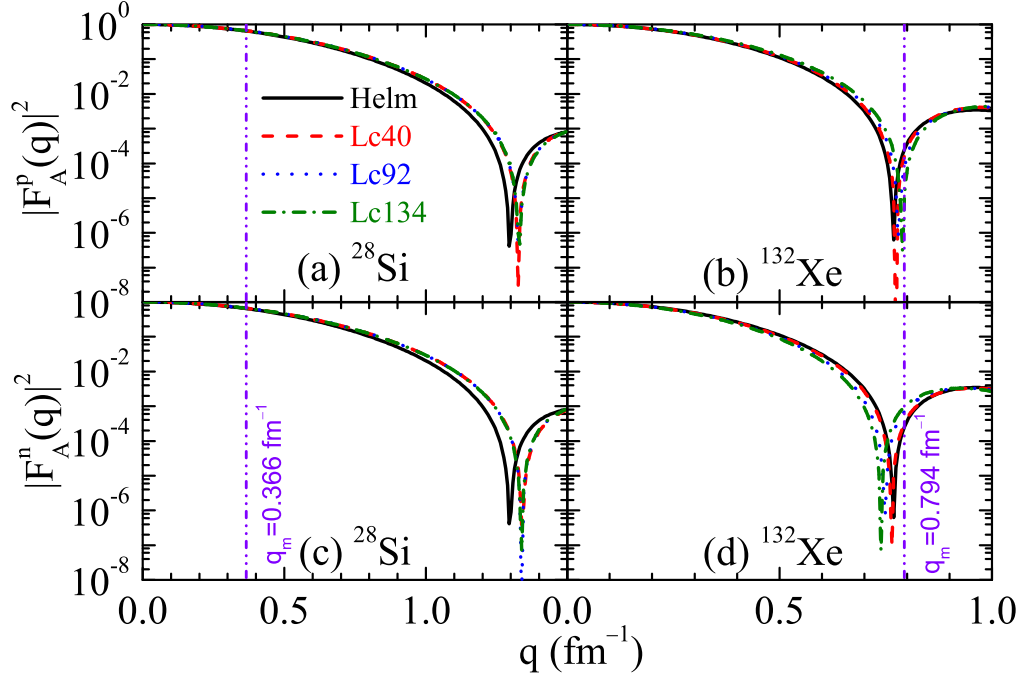


Figure 3: (Color online) Proton (upper panels) and neutron (lower panels) form factors as functions of momentum transfer q for ^{28}Si (left panels) and ^{132}Xe (right panels) obtained from SHF with Lc40, Lc92 and Lc134. The empirical Helm form factor is also included for comparison. The upper limit of the momentum transfer q_m , corresponding to a value of $E_R = 100$ keV, is indicated by dash-dot-dotted lines.

detection experiments, and the natural abundances of these elements are mostly dominated by their isotopes of ^{28}Si , ^{74}Ge and ^{132}Xe , respectively. Fig. 2 shows the relative deviation of the binding energies and charge rms radii of these nuclei from those measured in experiments [61–63]. It is seen that the interactions Lc40 and Lc92 can describe the experimental data very well (the deviations are within about $\pm 1\%$) except for the light nucleus ^{16}O for which the deviation of charge rms radius reaches to about 2.6%. It is interesting to see that, the interaction Lc134, which predicts a very strong density dependence of the symmetry energy at ρ_c and gives a very large neutron skin thickness of $\Delta r_{\text{np}} = 0.49$ fm for ^{208}Pb (the upper limit of the PREX measurement), still can give a reasonable description of the experimental data (the deviations are within about $\pm 2\%$ as indicated by bands in Fig. 2) except the nucleus ^{132}Sn for which the deviation of charge rms radius (binding energy) reaches to about -2.6% (3.7%) and for the light nucleus ^{16}O the deviation of charge rms radius is still about 2.6%. These results are remarkable as Lc40, Lc92 and Lc134 are not obtained from fitting measured binding energies and charge rms radii of finite nuclei as in usual Skyrme parametrization. It should be pointed out that our main motivation for introducing the Lc40, Lc92 and Lc134 is not to construct new Skyrme parameter sets to describe data, but to use them as references to study the symmetry energy effects in the following.

To investigate the symmetry energy effects on the proton and neutron distributions in finite nuclei, we plot in Fig. 3 the proton (upper panels) and neutron (lower panels) form factors as functions of momentum transfer q for ^{28}Si (left panels) and ^{132}Xe (right panels) from SHF calculations with Lc40, Lc92 and Lc134. For comparison, the results from the empirical Helm charge distributions (see Eq. (15)) are also included. In addition, also indicated in Fig. 3 is the upper limit of the momentum transfer q_m , corresponding to a value of $E_R = 100$ keV, which is commonly adopted in both experimental and theoretical studies [9, 36] and only events with the momentum transfer below q_m contribute to the analysis of the DM signals. It is seen from Fig. 3 that, for the nucleus ^{28}Si with equal proton and neutron numbers, the symmetry energy effect is tiny and the SHF calculations with Lc40, Lc92 and Lc134 predict almost the same form factors for neutrons and protons, which are further in good agreement with the empirical Helm charge form factor for $q \leq q_m$. On the other hand, for the neutron-rich nucleus ^{132}Xe , one can see a clear symmetry energy effect on the form factors, namely, a larger $L(\rho_c)$ shifts the neutron form factor to lower q values while shifts slightly the proton form factor to higher q values with the empirical Helm charge form factor in between, leading to an isospin splitting of the proton and neutron form factors with respect to the q value. These features actually reflect the symmetry energy effects on the neutron skin thickness, namely, increasing the value of $L(\rho_c)$ increases the rms radius of neutrons and reduces slightly the rms radius of protons, and thus leads to a larger neutron skin thickness as

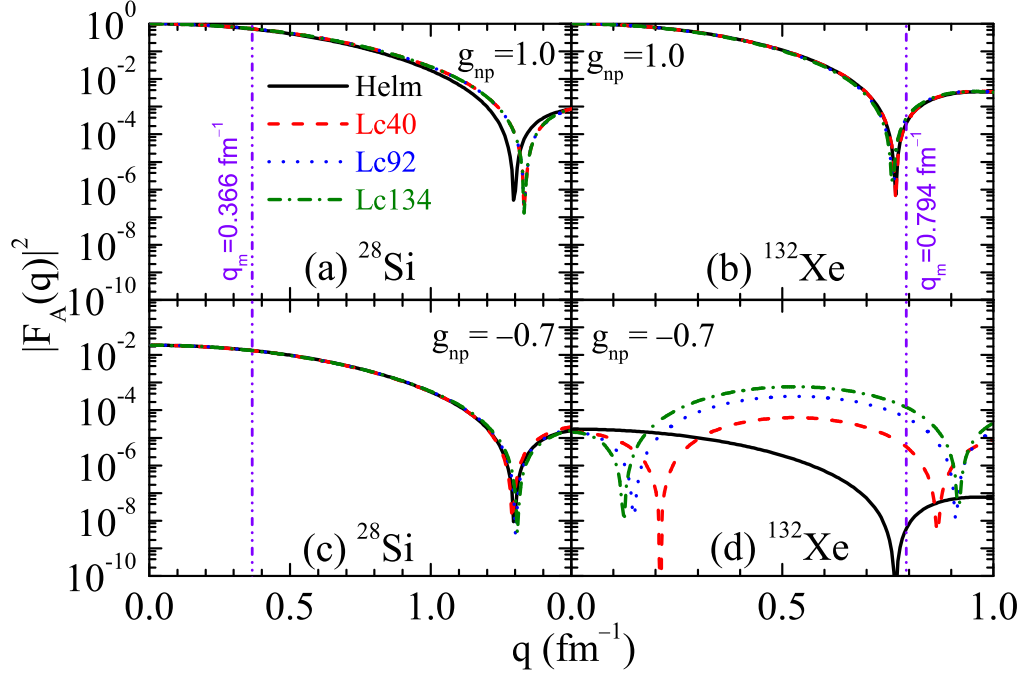


Figure 4: (Color online) Effective form factors as functions of momentum transfer q for ^{28}Si (left panels) and ^{132}Xe (right panels) with $g_{\text{np}} = 1.0$ (upper panels) and $g_{\text{np}} = -0.7$ (lower panels) obtained from SHF with Lc40, Lc92 and Lc134. The empirical Helm form factor is also included for comparison. The upper limit of the momentum transfer q_m , corresponding to a value of $E_R = 100$ keV, is indicated by dash-dot-dotted lines.

shown in Fig. 1.

Since the effective form factor (Eq. (11)) should be used to analyze the DM signals for general cases, it is expected that the isospin splitting of the proton and neutron form factors would cause significant effects on the effective form factor, especially for a negative g_{np} which could cause strongly destructive interference of DM scattering with protons and neutrons. This is illustrated in Fig. 4 where the effective form factor is plotted as a function of q for ^{28}Si (left panels) and ^{132}Xe (right panels) from SHF calculations with Lc40, Lc92 and Lc134. The results from the empirical Helm charge distributions with $F_A^{\text{p,n}}(q) = F_A^{\text{Helm}}(q)$ are also included for comparison. Also indicated in Fig. 4 is the upper limit of the momentum transfer q_m . In Fig. 4, two cases for the DM are considered: one is for the standard isospin-invariant DM with $g_{\text{np}} = 1.0$ (upper panels) and the other is for the IVDM with $g_{\text{np}} = -0.7$ (lower panels). It should be pointed out that $g_{\text{np}} = -0.7$, firstly suggested by Feng *et al.* [22], leads to nearly complete destructive interference of the scattering amplitudes for DM-proton and DM-neutron collisions for Xe-based detectors, and the IVDM with $g_{\text{np}} = -0.7$ is thus called as xenophobic DM [23]. For xenophobic DM, the confidence region of CDMS-II(Si) and the XENON100 exclusion contours are consistent with each other [32]. As will be shown later, for xenophobic DM, both the results from recent LUX [12] and the most recent SuperCDMS(Ge) [13] are also consistent with the confidence region of CDMS-II(Si). Theoretically, such negative values of g_{np} can arise, e.g., in models with a new light neutral gauge boson Z' [26, 30].

It is interesting to see from Fig. 4 that for $g_{\text{np}} = 1.0$, the effective form factors of both ^{28}Si and ^{132}Xe from SHF calculations with Lc40, Lc92 and Lc134 are in a very good agreement with the corresponding results from the empirical Helm charge distributions for $q \leq q_m$, indicating that there are essentially no symmetry energy effects. However, for $g_{\text{np}} = -0.7$, one can see that the effective form factors of ^{132}Xe display very different behaviors for different distributions, i.e., those from SHF calculations with Lc40, Lc92 and Lc134 as well as that from the empirical Helm charge distributions for $q \leq q_m$, although the effective form factors of ^{28}Si are essentially the same for these different distributions. These features indicate that the symmetry energy effect is tiny for the effective form factor of ^{28}Si but is very strong for that of ^{132}Xe in the case of $g_{\text{np}} = -0.7$. This is due to the fact that for a negative g_{np} , the scattering amplitudes for DM-proton and DM-neutron collisions may interfere destructively, and the DM particle is almost completely decoupled from the Xe isotopes, i.e. $F(q) \approx 0$ (see panel (d) of Fig. 4), especially when $g_{\text{np}} \approx -0.7$ [22]. In this case, a small difference between F_A^{p} and F_A^{n} may lead to a significant change for the effective form factor. As a result, the form factor of ^{132}Xe exhibits a very strong symmetry energy effect for $g_{\text{np}} = -0.7$, namely, a larger $L(\rho_c)$ value leads to a larger form factor for $0.15 \text{ fm}^{-1} \lesssim q \leq q_m$ as shown in panel (d) of Fig. 4. In

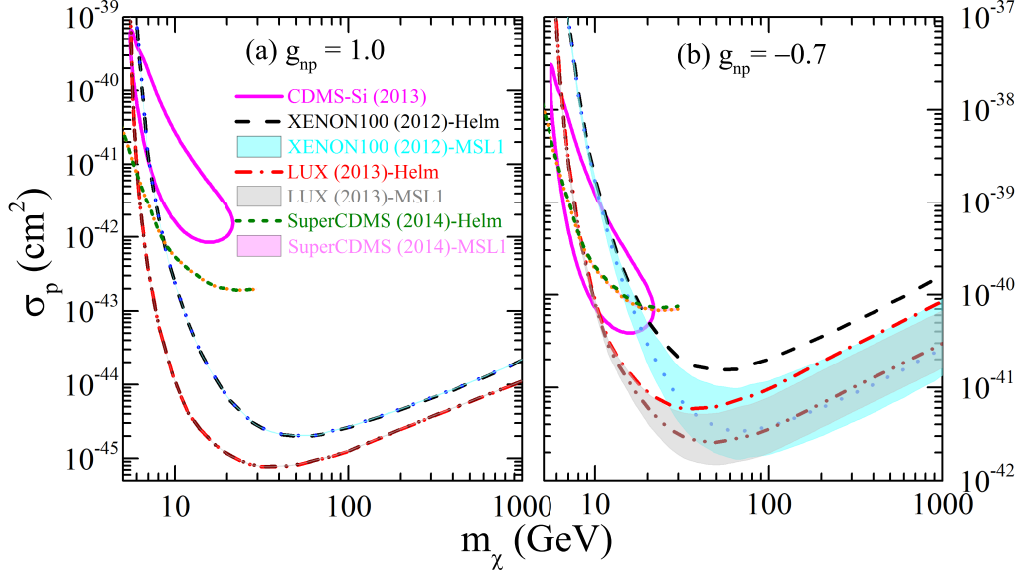


Figure 5: (Color online) Results of 90% confidence level (C.L.) limits from XENON100, LUX and SuperCDMS(Ge) together with 90% C.L. favored regions from CDMS-II(Si) in m_χ - σ_p plane for $g_{np} = 1.0$ (left panel) and $g_{np} = -0.7$ (right panel) with form factors from the empirical Helm charge distribution and SHF calculations with MSL1 by varying $L(\rho_c)$ from 40.5 MeV to 134.2 MeV.

particular, one can see that the effective form factors of ^{132}Xe from SHF calculations with Lc40, Lc92 and Lc134 can be significantly larger than that from the empirical Helm charge distributions for $0.3 \text{ fm}^{-1} \lesssim q \leq q_m$. This implies that the symmetry energy with a larger $L(\rho_c)$ (and thus a larger neutron skin thickness) can significantly enhance the effective DM-nucleus form factors in Eq. (7) when IVDM is considered. Therefore, one can expect a significant enhancement for the sensitivity of the Xe-based detectors to the DM-proton cross sections by taking into account of the symmetry energy effects with $g_{np} = -0.7$ in analyzing the experimental data.

B. Symmetry energy effects on the extraction of DM-proton cross sections

To see the effects of the symmetry energy and the isospin-violation factor g_{np} on the extracted spin-independent DM-proton cross sections σ_p in DM direct detection experiments, we show in Fig. 5 the results of the 90% confidence level (C.L.) limits from XENON100 [11], LUX [12] and SuperCDMS(Ge) [13] along with the 90% C.L. favored regions from CDMS-II(Si) [8] in DM mass m_χ - σ_p plane for $g_{np} = 1.0$ (left panel) and $g_{np} = -0.7$ (right panel) with form factors from the empirical Helm charge distribution and SHF calculations with MSL1 by varying $L(\rho_c)$ from 40.5 MeV to 134.2 MeV. For the results from SuperCDMS(Ge), only the mass region less than 30 GeV is shown since no data are available for $m_\chi > 30$ GeV [13]. In these analyses, we use the standard astrophysical parameters in the Standard Halo Model, namely, a Maxwell-Boltzmann distribution for $f(v)$ with $v_0 = 220$ km/s and Galactic escape velocity $v_{\text{esc}} = 544$ km/s, and a DM density of $\rho_\chi = 0.3 \text{ GeV/cm}^3$ [64].

For the isospin-invariant DM with $g_{np} = 1.0$, one can see from Fig. 5 that CDMS-II(Si) results are in some tension with the upper limit placed by the XENON100 experiment, and they become in even strong disagreement with the upper limits set by the recent LUX [12] experiment and the more recent SuperCDMS(Ge) [13] experiment. However, for the IVDM with $g_{np} = -0.7$, one can see that the tension between CDMS-II(Si) and XENON100 is essentially disappeared as found by Frandsen *et al.* [32]. Furthermore, it is remarkable to see from the right panel of Fig. 5 that the disagreement of the CDMS-II(Si) results with LUX and SuperCDMS(Ge) can also be largely ameliorated within the framework of IVDM with $g_{np} = -0.7$ [66]. Therefore, these results indicate that the IVDM indeed provides a very promising mechanism to reconcile the tension among various experiments.

Furthermore, it is interesting to see that, although there are essentially no symmetry energy effects on the extracted spin-independent DM-proton cross sections σ_p in different experiments in the case of isospin-invariant DM with $g_{np} = 1.0$, the symmetry energy effects can significantly affect the extraction of σ_p for the Xe-based experiments (XENON100 and LUX) in the case of IVDM with $g_{np} = -0.7$. Therefore, our results indicate that, for isospin-invariant DM, the widely used empirical Helm form factor is well grounded and this is consistent with our previous discussions about the form factors. On the other hand, for IVDM with $g_{np} = -0.7$, using the form factors obtained

from SHF calculations in MSL1 with varied $L(\rho_c)$ values generally increases the sensitivity of the Xe-based detectors (XENON100 and LUX) compared with using the empirical Helm form factor, and a larger $L(\rho_c)$ value, which leads to a larger neutron skin thickness in Xe isotopes, generally leads to a stronger sensitivity of the Xe-based detectors. This symmetry energy effect becomes more pronounced with the increment of the DM mass m_χ . While the symmetry energy effect is about 20% for the DM mass of $m_\chi \approx 8$ GeV, it can become very significant for the DM with mass above a few tens GeV. For $m_\chi = 20$ GeV, which roughly corresponds to the DM mass upper limit of CDMS-II(Si) bounds, the sensitivities of XENON100 and LUX can be enhanced by a factor of 3 using the form factor with $L(\rho_c) = 134.2$ MeV compared with that using the empirical Helm form factor. In particular, the sensitivities can have a factor of more than 10 improvement for $m_\chi \geq 80$ GeV where many constraints for supersymmetric WIMPs have been put by the data from LHC [65]. On the other hand, the relative variation between the results extracted from the Helm form factor and the SHF calculations is small ($< 7\%$) for SuperCDMS(Ge) and it can be negligible ($< 0.5\%$) for CDMS-II(Si) for which the results from the SHF calculations are not shown in Fig. 5.

The DM mass dependence of the symmetry energy effects observed in XENON100 and LUX for $g_{np} = -0.7$ can be understood as a result of the v_{\min} effects in the velocity integration of Eq. (14) together with the enhancement effects of the form factors caused by taking into account of the symmetry energy as discussed in the previous subsection. More specifically, for a fixed recoil energy, the larger the DM mass m_χ is, the smaller the v_{\min} is (see Eq. (8)). Since the local DM velocity distribution $f(v)$ is fixed as a specified Maxwell-Boltzmann distribution, a smaller v_{\min} means a larger value of the velocity integration $k(E_R, m_\chi)$ in Eq. (13) and this will significantly enhance the effects caused by different form factors adopted for the E_R integration in the numerator of r.h.s of Eq. (13).

It is also very interesting to see that for the case with $g_{np} = -0.7$, the curves of XENON100 and LUX overlap with each other in the mass region larger than about 70 GeV in the right panel of Fig. 5. This can be explained as a combined result of the form factor effect due to the symmetry energy which can increase significantly the sensitivity of Xe-based detectors and the different threshold energy cuts set by XENON100 and LUX experiments. Particularly, the form factor effect is dominated by the events with a larger recoil energy, i.e., a larger momentum transfer as shown in Fig. 4(d). Since the energy range of $3.0 - 22.1$ keV adopted by LUX [12] rules out the events with larger recoil energies compared to XENON100 which adopts a larger energy range of $6.6 - 43.3$ keV [11], the form factor effect in XENON100 is thus more significant than that in LUX. This effect becomes more important with the increment of the DM mass. As a result, the limits set by XENON100 and LUX overlap with each other for larger DM masses even though LUX provides much more stringent limit on the spin-independent elastic DM-proton scattering cross section in the isospin-invariant case with $g_{np} = 1.0$ as shown in Fig. 5 (a). It should be mentioned that the small symmetry energy effect observed for SuperCDMS(Ge) in Fig. 5 (b) is partially due to the smaller threshold energy cut, i.e., $1.6 - 10.0$ keV [13].

C. Symmetry energy effects with various isospin-violation factor g_{np}

As mentioned earlier, for IVDM with $g_{np} = -0.7$, the sensitivity of Xe-based detectors is highly suppressed and the tension among various experiments using different target elements can be largely ameliorated. Following the method by Feng *et al.* [23], we further study in the following how the symmetry energy effects change for various isospin-violation factor g_{np} . Shown in Fig. 6 is the degradation factor D_p (see Eq. (13)) as a function of the isospin-violation factor g_{np} obtained by using the empirical Helm form factors as well as the form factors from SHF calculations with different symmetry energies constrained by PREX experiment, i.e., Lc40, Lc92 and Lc134, for $m_\chi = 8$ GeV (panel (a)) and $m_\chi = 100$ GeV (panel (b)). Since both XENON100 and LUX are Xe-based experiments and they have similar dependence on the g_{np} and the symmetry energy, we thus consider CDMS-II(Si), SuperCDMS(Ge) and XENON100 in Fig. 6. In addition, for $m_\chi = 100$ GeV, the symmetry energy effect is negligible for CDMS-II(Si) and relatively small for SuperCDMS(Ge) which adopts a small threshold energy cut and has been designed especially for light DM searching, we thus only show the results of XENON100 (panel (b)).

It is seen from Fig. 6 that generally the sensitivity of each detector is significantly suppressed for a negative g_{np} within the range of $-1.0 < g_{np} < -0.5$ due to destructive interference between DM-neutron and DM-proton scattering amplitudes as pointed out in Ref. [22, 23]. However, the D_p reaches its minimum value (where the detector is most insensitive) at different values of g_{np} for different detectors due to the different compositions and distributions of neutrons and protons in each target element of the detector. In particular, one can see that the corresponding value of g_{np} which leads to a minimum value of D_p , denoted as g_{np}^{\min} , is about -0.993 , -0.787 and -0.700 for CDMS-II(Si), SuperCDMS(Ge) and XENON100, respectively, for the case of $m_\chi = 8$ GeV when the empirical Helm form factor is used. For $m_\chi = 8$ GeV, the symmetry energy effect is very small for CDMS-II(Si) and the largest relative variation with $L(\rho_c)$ varied from 40.2 MeV to 134.2 MeV with respect to the results from the empirical Helm form factor is 1.26% at $g_{np} = -0.997$. The largest relative variation due to the symmetry energy effect is 6.22% at $g_{np} = -0.818$ for SuperCDMS(Ge), and it becomes 47.11% at $g_{np} = -0.686$ for XENON100. As a matter of fact, a clear shift for

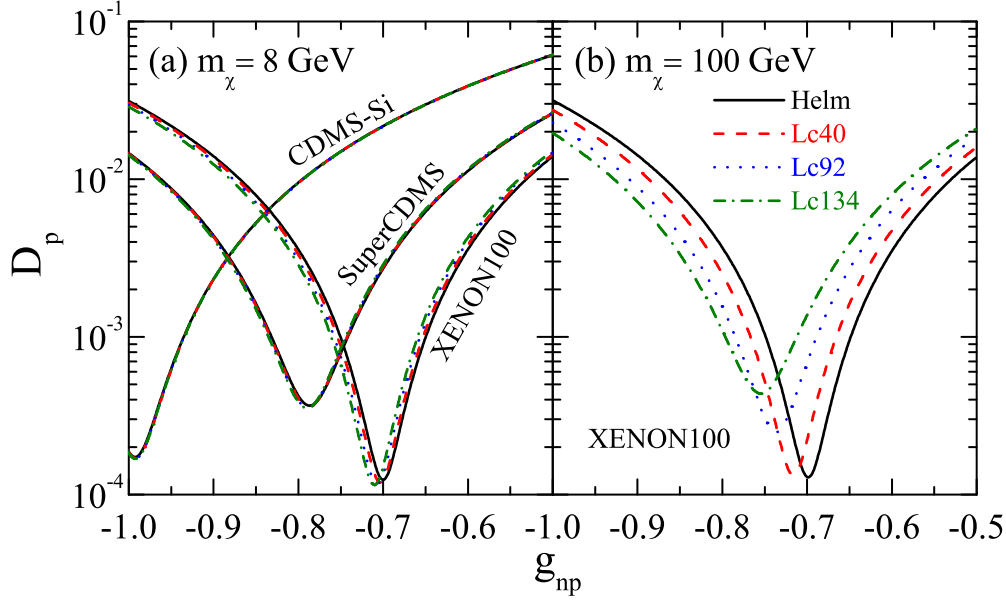


Figure 6: (Color online) Degradation factor D_p as a function of the isospin-violation factor g_{np} obtained by using the empirical Helm form factors as well as the form factors from SHF calculations with Lc40, Lc92 and Lc134 for $m_\chi = 8$ GeV (panel (a)) and $m_\chi = 100$ GeV (panel (b)). For $m_\chi = 8$ GeV, the results of CDMS-II(Si), SuperCDMS(Ge) and XENON100 are shown while only the results of XENON100 are shown for $m_\chi = 100$ GeV.

curves for the Xe-based detectors calculated with different symmetry energies has been already seen even for such a small DM mass in Fig. 6 (a). These features indicate that the symmetry energy effect can be already pronounced for XENON100 even for a small mass DM with $m_\chi = 8$ GeV. For XENON100, one can see from Fig. 6(b) that the symmetry energy effect becomes very strong for $m_\chi = 100$ GeV. In particular, a larger $L(\rho_c)$ value gives significantly stronger sensitivity of the detectors and the largest relative variation due to the symmetry energy effect is 952.30% (almost one order) at $g_{np} = -0.695$. Furthermore, one can see the value of g_{np}^{\min} also depends significantly on the symmetry energy, and it is -0.716 , -0.737 and -0.754 for $L(\rho_c) = 40.2$, 92.4 and 134.2 MeV, respectively. It is interesting to see that one cannot find a g_{np} value such that $D_p \rightarrow 0$, leading to zero sensitivity for scattering off the elements, and this is mainly due to the fact that the elements have multiple isotopes and completely destructive interference cannot be simultaneously achieved for all isotopes [22, 23]. We would like to point out that even for elements with only one naturally abundant isotope, one still cannot find a g_{np} value such that $D_p \rightarrow 0$ since the neutron form factor is generally different from the proton form factor in a nucleus.

These features indicates that, the symmetry energy effect can not only improve the sensitivities of the detectors, but also affect the interaction behaviors of the target element with the isospin-violating DM in various isospin-violating regions we are interested in for DM direct detection experiments. In future when different direct detection experiments using various target elements had specify the DM signals precisely, one may determine simultaneously the isospin-violation factor g_{np} and the symmetry energy, especially if the IVDM particle has a larger mass of above tens of GeV. Our results also imply that the DM-nucleus scattering provides a potential useful model-independent tool to determine the neutron distribution in nuclei if DM is xenophobic IVDM.

IV. CONCLUSION

In the present work, we have shown that isospin-violating dark matter (IVDM) indeed provides a possible mechanism to ameliorate the tension among recent direct detection experiments, including CDMS-II(Si), XENON100, LUX, and SuperCDMS(Ge). For IVDM, we have demonstrated that the results of the DM direct detection experiments based on neutron-rich target nuclei, e.g., Xe-based detector, may strongly depend on the neutron skin thickness of the target nuclei, which characterizes the relative difference of neutron and proton distributions in the nuclei. Experimentally, the neutron skin thickness is poorly known mainly due to the large uncertainties of the neutron distributions. Theoretically, it has been established that the neutron skin thickness is determined uniquely by the density slope $L(\rho_c)$ of the symmetry energy at a subsaturation cross density $\rho_c \approx 0.11 \text{ fm}^{-3}$. Therefore, the symmetry

energy effects can play an important role in analyzing the DM signals in this case.

In particular, using the proton and neutron distributions obtained from Skyrme-Hartree-Fock calculations with the $L(\rho_c)$ constrained by the latest model-independent measurement of the neutron skin thickness from PREX experiment at JLab, we have found that although the symmetry energy effects on the extracted bounds on DM-proton cross sections are negligible in the direct detection for isospin-invariant DM, they could become critically important in the detection for IVDM. Especially, for the xenophobic IVDM in the mass region constrained by CMDS-II(Si), the symmetry energy effect may enhance the sensitivity of Xe-based detectors (e.g., XENON100 and LUX) to the DM-proton cross section by a factor of 3, compared with the results using the empirical Helm nuclear form factors extracted from empirical charge distributions. This symmetry energy effect can even enhance the sensitivity by more than a factor of 10 for the xenophobic IVDM with mass larger than 80 GeV. Our results imply that the DM-nucleus scattering provides a potentially useful model-independent tool to determine the neutron distribution in nuclei and thus the density dependence of the symmetry energy if DM is indeed xenophobic IVDM.

Acknowledgments

The authors would like to thank Fei Gao for useful discussions. This work was supported in part by the NNSF of China under Grant Nos. 11275125 and 11135011, the Shanghai Rising-Star Program under grant No. 11QH1401100, the “Shu Guang” project supported by Shanghai Municipal Education Commission and Shanghai Education Development Foundation, the Program for Professor of Special Appointment (Eastern Scholar) at Shanghai Institutions of Higher Learning, and the Science and Technology Commission of Shanghai Municipality (11DZ2260700).

-
- [1] **Planck** Collaboration, P. A. R. Ade et al., *Planck 2013 results. XVI. Cosmological parameters*, arXiv:1303.5076.
 - [2] G. Steigman and M. S. Turner, *Cosmological Constraints on the Properties of Weakly Interacting Massive Particles*, *Nucl. Phys. B* **253** (1985) 375.
 - [3] G. Jungman, M. Kamionkowski, and K. Griest, *Supersymmetric dark matter*, *Phys. Rept.* **267** (1996) 195 [hep-ph/9506380].
 - [4] M. W. Goodman and E. Witten, *Detectability of Certain Dark Matter Candidates*, *Phys. Rev. D* **31** (1985) 3059.
 - [5] **CoGeNT** Collaboration, C. E. Aalseth et al., *Results from a Search for Light-Mass Dark Matter with a P-type Point Contact Germanium Detector*, *Phys. Rev. Lett.* **106** (2011) 131301 [arXiv:1002.4703].
 - [6] C. Savage et al., *Compatibility of DAMA/LIBRA dark matter detection with other searches*, *JCAP* **0904** (2009) 010 [arXiv:0808.3607].
 - [7] **CRESST II** Collaboration, G. Angloher et al., *Results from 730 kg days of the CRESST-II Dark Matter Search*, *European Physical Journal C* **72** (2012) 1971 [arXiv:1109.0702].
 - [8] **CDMS II** Collaboration, R. Agnese et al., *Silicon Detector Results from the First Five-Tower Run of CDMS II*, *Phys. Rev. D* **88** (2013) 031104 [arXiv:1304.3706].
 - [9] **CDMS II** Collaboration, R. Agnese et al., *Dark Matter Search Results Using the Silicon Detectors of CDMS II*, *Phys. Rev. Lett.* **111** (2013) 251301 [arXiv:1304.4279].
 - [10] **XENON100** Collaboration, E. Aprile et al., *Dark Matter Results from 100 Live Days of XENON100 Data*, *Phys. Rev. Lett.* **107** (2011) 131302 [arXiv:1104.2549].
 - [11] **XENON100** Collaboration, E. Aprile et al., *Dark Matter Results from 225 Live Days of XENON100 Data*, *Phys. Rev. Lett.* **109** (2012) 181301 [arXiv:1207.5988].
 - [12] **LUX** Collaboration, D.S. Akerib et al., *First results from the LUX dark matter experiment at the Sanford Underground Research Facility*, *Phys. Rev. Lett.* **112** (2014) 091303 [arXiv:1310.8214].
 - [13] **SuperCDMS** Collaboration, R. Agnese et al., *Search for Low-Mass WIMPs with SuperCDMS*, arXiv:1402.7137.
 - [14] C. Savage, G. Gelmini, P. Gondolo, and K. Freese, *XENON10/100 dark matter constraints in comparison with CoGeNT and DAMA: Examining the L_{eff} dependence*, *Phys. Rev. D* **83** (2011) 055002 [arXiv:1006.0972].
 - [15] D. Smith and N. Weiner, *Inelastic dark matter*, *Phys. Rev. D* **64** (2001) 043502 [arXiv:hep-ph/0101138].
 - [16] M. T. Frandsen, F. Kahlhoefer, C. McCabe, S. Sarkar, and K. Schmidt-Hoberg, *Resolving astrophysical uncertainties in dark matter direct detection*, *JCAP* **024** (2012) 1201 [arXiv:1111.0292].
 - [17] Y.-Y. Mao, L. E. Strigari, and R. H. Wechsler, *Connecting Direct Dark Matter Detection Experiments to Cosmologically Motivated Halo Models*, *Phys. Rev. D* **89** (2014) 063513 [arXiv:1304.6401].
 - [18] R. C. Cotta, A. Rajaraman, T. M. P. Tait, and A. M. Wijangco, *Particle Physics Implications and Constraints on Dark Matter Interpretations of the CDMS Signal*, arXiv:1305.6609.
 - [19] A. Kurylov and M. Kamionkowski, *Generalized analysis of weakly interacting massive particle searches*, *Phys. Rev. D* **69** (2004) 063503 [hep-ph/0307185].
 - [20] F. Giuliani, *Are direct search experiments sensitive to all spin-independent WIMP candidates?*, *Phys. Rev. Lett.* **95** (2005) 101301 [hep-ph/0504157].
 - [21] S. Chang, J. Liu, A. Pierce, N. Weiner and I. Yavin, *CoGeNT Interpretations*, *JCAP* **08** (2010) 018 [arXiv:1004.0697].

- [22] J. L. Feng, J. Kumar, D. Marfatia, D. Sanford, *Isospin-Violating Dark Matter*, *Phys. Lett. B* **703** (2011) 124-127 [arXiv:1102.4331].
- [23] J. L. Feng, J. Kumar, and D. Sanford, *Xenophobic Dark Matter*, *Phys. Rev. D* **88** (2013) 015021 [arXiv:1306.2315].
- [24] J. L. Feng, J. Kumar, D. Marfatia, and D. Sanford, *Isospin-Violating Dark Matter Benchmarks for Snowmass 2013*, arXiv:1307.1758.
- [25] K. I. Nagao and T. Naka, *Isospin-violating dark matter search by nuclear emulsion detector*, *Prog. Theor. Exp. Phys. B* **02** (2013) 043 [arXiv:1205.0198].
- [26] M. T. Frandsen, F. Kahlhoefer, S. Sarkar, and K. Schmidt-Hoberg, *Direct detection of dark matter in models with a light Z*, *JHEP* **1109** (2011) 128 [arXiv:1107.2118].
- [27] J. M. Cline and A. R. Frey, *Minimal hidden sector models for CoGeNT/DAMA events*, *Phys. Rev. D* **84** (2011) 075003 [arXiv:1108.1391].
- [28] E. Del Nobile, C. Kouvaris, F. Sannino, and J. Virkajarvi, *Dark Matter Interference*, *Mod. Phys. Lett. A* **27** (2012) 1250108 [arXiv:1111.1902].
- [29] X.-G. He, B. Ren, and J. Tandean, *Hints of standard model Higgs boson at the LHC and light dark matter searches*, *Phys. Rev. D* **85** (2012) 093019 [arXiv:1112.6364].
- [30] X. Gao, Z. Kang, and T. Li, *Origins of the isospin violation of dark matter interactions*, *JCAP* **01** (2013) 021 [arXiv:1107.3529].
- [31] J. D. Lewin and P. F. Smith, *Review of mathematics, numerical factors, and corrections for dark matter experiments based on elastic nuclear recoil*, *Astroparticle Phys.* **6** (1996) 87.
- [32] M. T. Frandsen et al., *The unbearable lightness of being: CDMS versus XENON*, *JCAP* **07** (2013) 023 [arXiv:1304.6066].
- [33] R. Helm, *Inelastic and Elastic Scattering of 187-Mev Electrons from Selected Even-Even Nuclei*, *Phys. Rev.* **104** (1956) 1466.
- [34] G. Duda, A. Kemper, and P. Gondolo, *Model Independent Form Factors for Spin Independent Neutralino-Nucleon Scattering from Elastic Electron Scattering Data*, *JCAP* **0704** (2007) 012 [hep-ph/0608035].
- [35] Y.Z. Chen, Y.Z. Luo, L. Li, H. Shen, and X.Q. Li, *Determining Nuclear Form factor for Detection of Dark Matter in Relativistic Mean Field Theory*, *Commun. Ther. Phys.* **55** (2011) 1059 [arXiv:1101.3049].
- [36] G. Go', V. De Donno, M. Anguiano and A.M. Lallena, *Nuclear proton and neutron distributions in the detection of weak interacting massive particles*, *JCAP* **11** (2012) 010 [arXiv:1211.1787].
- [37] R. Hofstadter, *Electron scattering and nuclear structure*, *Rev. Mod. Phys.* **28** (1956) 214.
- [38] B. Frois et al., *High Momentum Transfer electron Scattering from Pb-208*, *Phys. Rev. Lett.* **38** (1977) 152.
- [39] C. W. de Jager and C. de Vries, *Nuclear charge-density-distributions parameters*, *At. Data Nucl. Data Tables* **36** (1987) 495.
- [40] **PREX** Collaboration, S. Abrahamyan et al., *Measurement of the Neutron Radius of 208Pb Through Parity-Violation in Electron Scattering*, *Phys. Rev. Lett.* **108** (2012) 112502 [arXiv:1201.2568].
- [41] A. Ong, J. C. Berengut, and V. V. Flambaum, *The Effect of spin-orbit nuclear charge density corrections due to the anomalous magnetic moment on halonuclei*, *Phys. Rev. C* **82** (2010) 014320 [arXiv:1006.5508].
- [42] C.J. Horowitz et al., *Neutron star structure and the neutron radius of Pb-208*, *Phys. Rev. Lett.* **86** (2001) 5647 [astro-ph/0010227].
- [43] B.A. Brown, *Neutron radii in nuclei and the neutron equation of state*, *Phys. Rev. Lett.* **85** (2000) 5296; S. Typel and B.A. Brown, *Neutron radii and the neutron equation of state in relativistic models*, *Phys. Rev. C* **64** (2001) 027302.
- [44] B.A. Li, L.W. Chen, and C.M. Ko, *Recent Progress and New Challenges in Isospin Physics with Heavy-Ion Reactions*, *Phys. Rep.* **464** (2008) 113 [arXiv:0804.3580].
- [45] Z. Zhang and L.W. Chen, *Constraining the symmetry energy at subsaturation densities using isotope binding energy difference and neutron skin thickness*, *Phys. Lett. B* **726** (2012) 234 [arXiv:1302.5327].
- [46] Topical Issue *Nuclear Symmetry Energy* edited by Bao-An Li, 'Angels Ramos, Giuseppe Verde, Isaac Vidana, *Eur. Phys. J. A* **50** (2014).
- [47] E. Chabanat, P. Bonche, P. Haensel, J. Meyer, and R. Schaeffer, *A Skyrme parametrization from subnuclear to neutron star densities*, *Nucl. Phys. A* **627** (1997) 710.
- [48] J. Friedrich and P.-G. Reinhard, *Skyrme-force parametrization: Least-squares fit to nuclear ground-state properties*, *Phys. Rev. C* **33** (1986) 335.
- [49] P. Klüpfel, P.-G. Reinhard, T.J. Bürvenich, and J.A. Maruhn, *Variations on a theme by Skyrme: A systematic study of adjustments of model parameters*, *Phys. Rev. C* **79** (2009) 034310 [arXiv:0804.3385].
- [50] L.W. Chen, C.M. Ko, B.A. Li, and J. Xu, *Density slope of the nuclear symmetry energy from the neutron skin thickness of heavy nuclei*, *Phys. Rev. C* **82** (2010) 024321 [arXiv:1004.4672].
- [51] L.W. Chen and J.Z. Gu, *Correlations between the nuclear breathing mode energy and properties of asymmetric nuclear matter*, *J. Phys. G* **39** (2012) 035104 [arXiv:1104.5407].
- [52] L.W. Chen, *Higher order bulk characteristic parameters of asymmetric nuclear matter*, *Sci. China: Phys. Mech. Astro.* **54** (Suppl. 1) (2011) s124 [arXiv:1101.2384].
- [53] L.W. Chen, *Nuclear matter symmetry energy and the symmetry energy coefficient in the mass formula*, *Phys. Rev. C* **83** (2011) 044308 [arXiv:1101.5217].
- [54] G. Gelmini and P. Gondolo, *WIMP annual modulation with opposite phase in Late-Infall halo models*, *Phys. Rev. D* **64** (2001) 023504 [hep-ph/0012315].
- [55] R. Schoenrich, J. Binney, and W. Dehnen, *Local Kinematics and the Local Standard of Rest*, *Mon. Not. R. Astron. Soc.* **403** (2010) 1829.

- [56] P. Ring and P. Schuck, *The nuclear many-body problem*, Springer, Berlin, 1980.
- [57] R. Chen, B.J. Cai, L.W. Chen, B.A. Li, C. Xu, and J. Xu, *Single-nucleon potential decomposition of the nuclear symmetry energy*, *Phys. Rev. C* **85** (2012) 024305 [arXiv:1112.2936].
- [58] L.W. Chen, C.M. Ko, and B.A. Li, *Isospin-dependent properties of asymmetric nuclear matter in relativistic mean field models*, *Phys. Rev. C* **76** (2007) 054316 [arXiv:0709.0900].
- [59] F.J. Fattoyev, C.J. Horowitz, J. Piekarewicz, and G. Shen, *Relativistic effective interaction for nuclei, giant resonances, and neutron stars*, *Phys. Rev. C* **82** (2010) 055803 [arXiv:1008.3030].
- [60] F.J. Fattoyev and J. Piekarewicz, *Has a Thick Neutron Skin in Pb208 Been Ruled Out?*, *Phys. Rev. Lett.* **111** (2013) 162501 [arXiv:1306.6034].
- [61] M. Wang, G. Audi, A. H. Wapstra, F. G. Kondev, M. MacCormick, X. Xu, and B. Pfeiffer, *The Ame2012 atomic mass evaluation (II). Tables, graphs and references*, *Chin. Phys. C* **36** (2012) 1287.
- [62] I. Angeli, *A consistent set of nuclear rms charge radii: properties of the radius surface $R(N,Z)$* , *At. Data Nucl. Data Tab.* **87** (2004) 185.
- [63] F. Le Blanc, L. Cabaret, E. Cottureau, J.E. Crawford, S. Essabaa, J. Genevey, R. Horn, G. Huber, J. Lassen, J.K.P. Lee, G. Le Scornet, J. Lettry, J. Obert, J. Oms, A. Ouchrif, J. Pinard, H. Ravn, B. Roussiere, J. Sauvage, and D. Verney, *Charge-radius change and nuclear moments in the heavy tin isotopes from laser spectroscopy: Charge radius of ^{132}Sn* , *Phys. Rev. C* **72** (2005) 034305.
- [64] M. C. Smith et al., *The RAVE Survey: Constraining the Local Galactic Escape Speed*, *Mon. Not. R. Astron. Soc.* **379** (2007) 755 [astro-ph/0611671].
- [65] C. Strey et al., *Updated global fits of the $m\overline{SSM}$ including the latest LHC SUSY and Higgs searches and XENON100 data*, *JCAP* **1203** (2012) 030 [arXiv:1112.4192]; A. Fowlie, M. Kazana, K. Kowalska, S. Munir, L. Roszkowski, E. Sessolo, S. Trojanowski, and Y.-L. Tsai, *The $m\overline{SSM}$ Favoring New Territories: The Impact of New LHC Limits and a 125 GeV Higgs*, *Phys. Rev. D* **86** (2012) 075010 [arXiv:1206.0264]; O. Buchmueller et al., *Higgs and Supersymmetry*, *Eur. Phys. J. C* **72** (2012) 2020 [arXiv:1112.3564].
- [66] Koichi Hamaguchi, Seng Pei Liew, Takeo Moroi, Yasuhiro Yamamoto, *Isospin-Violating Dark Matter with Colored Mediators*, arXiv:1403.0324.